

Melanin-Targeted Preclinical PET Imaging of Melanoma Metastasis

Gang Ren¹, Zheng Miao¹, Hongguang Liu¹, Lei Jiang¹, Naengnoi Limpa-Amara², Ashfaq Mahmood², Sanjiv S. Gambhir¹, and Zhen Cheng¹

¹Molecular Imaging Program at Stanford (MIPS), Department of Radiology and Bio-X Program, Stanford University, Stanford, California; and ²Division of Nuclear Medicine, Department of Radiology, Harvard Medical School and Brigham and Women's Hospital, Boston, Massachusetts

Dialkylamino-alkyl-benzamides possess an affinity for melanin, suggesting that labeling of such benzamides with ¹⁸F could potentially produce melanin-targeted PET probes able to identify melanotic melanoma metastases in vivo with high sensitivity and specificity. **Methods:** In this study, *N*-[2-(diethylamino)-ethyl]-4-¹⁸F-fluorobenzamide (¹⁸F-FBZA) was synthesized via a 1-step conjugation reaction. The α -receptor binding affinity of ¹⁹F-FBZA was determined along with the in vitro cellular uptake of radiofluorinated ¹⁸F-FBZA in B16F10 cells. In vivo distribution and small-animal PET studies were conducted on mice bearing B16F10 melanoma, A375M amelanotic melanoma, and U87MG tumors, and comparative studies were performed with ¹⁸F-FDG PET in the melanoma models. **Results:** In vitro, uptake of ¹⁸F-FBZA was significantly higher in B16F10 cells treated with L-tyrosine ($P < 0.001$). In vivo, ¹⁸F-FBZA displayed significant tumor uptake; at 2 h, 5.94 ± 1.83 percentage injected dose (%ID) per gram was observed in B16F10 tumors and only 0.75 ± 0.09 %ID/g and 0.56 ± 0.13 %ID/g was observed in amelanotic A375M and U87MG tumors, respectively. Lung uptake was significantly higher in murine lungs bearing melanotic B16F10 pulmonary metastases than in normal murine lungs ($P < 0.01$). Small-animal PET clearly identified melanotic lesions in both primary and pulmonary metastasis B16F10 tumor models. Co-registered micro-CT with small-animal PET along with biopsies further confirmed the presence of tumor lesions in the mouse lungs. **Conclusion:** ¹⁸F-FBZA specifically targets primary and metastatic melanotic melanoma lesions with high tumor uptake and may have translational potential.

Key Words: malignant melanoma; melanin; PET; imaging; ¹⁸F

J Nucl Med 2009; 50:1692–1699

DOI: 10.2967/jnumed.109.066175

Malignant melanoma is one of the most lethal cancers because of its high systemic metastatic potential. The incidence of this disease has doubled over the past 2 decades and is continually increasing, making it a significant public health problem in Europe and the United States

(1,2). Currently, although regimens for effective treatment of melanoma are still not available, increased surveillance with early diagnosis and accurate staging of the disease is an important approach to increasing survival. PET offers the promise of noninvasively imaging micrometastases (3,4) but must be coupled with an appropriate probe to provide oncologists with highly sensitive detection of metastases and accurate staging of high-risk melanomas.

Through imaging of different tumor molecular targets and pathways, several PET probes, including ¹⁸F-FDG (3–5), 6-¹⁸F-fluoro-L-dihydroxyphenylalanine (6), L-[methyl-¹¹C]methionine (7), 3'-¹⁸F-fluoro-3'-deoxy-L-thymidine (8), ¹⁸F-galacto-RGD peptide (9), and others, have been evaluated for melanoma detection in patients. However, reports suggest that the overall detection rate has been "extremely low" for occult metastatic lesions in patients with stage IB or II melanoma using ¹⁸F-FDG PET/CT (5). ¹⁸F-FDG also failed to identify metastatic lesions smaller than 1 cm in diameter located mainly in common sites for melanoma metastases: the lungs, liver, or brain (3). Moreover, the molecular targets for ¹⁸F-FDG are glucose transporters (e.g., glucose transporter 1) and hexokinase, which relate to the glycolytic activity of tumors (10). Novel PET probes with a higher specificity and sensitivity for other molecular targets and biologic processes in melanoma are still highly desired for visualizing and monitoring their expression and activity or for detecting small lesions and metastases.

Melanin is an amorphous, irregular polymer comprising mixtures of 2 separate but biogenetically related pigments, eumelanins and phenomelanins (11,12). Melanin biosynthesis is an essential metabolic pathway regulated by tyrosinase activity in melanocytes (13). In malignant melanoma, melanin formation is highly increased because tyrosinase activity is significantly elevated (12,14). Taking advantage of the unique physiologic process of melanin synthesis, many studies have developed melanin-targeted radiotherapeutic and chemotherapeutic (15–17) agents for melanoma treatment. Benzamide analogs possess selective affinities with melanin and, over the past 2 decades, have been extensively investigated for development of SPECT

Received May 19, 2009; revision accepted Jun. 30, 2009.

For correspondence or reprints contact: Zhen Cheng, Molecular Imaging Program at Stanford, Department of Radiology, 1201 Welch Rd., Lucas Expansion, P020A, Stanford University, Stanford, CA 94305.

E-mail: zcheng@stanford.edu

COPYRIGHT © 2009 by the Society of Nuclear Medicine, Inc.

agents for melanoma detection. Many benzamide analogs exhibit excellent in vivo tumor-targeting profiles. It was reported that *N*-(2-diethylaminoethyl)-4-¹²⁵I-iodo-benzamide (¹²⁵I-BZA) displayed uptake of 6.75 ± 0.67 percentage injected dose per gram (%ID/g) at 1 h in the tumors of C57BL6 mice bearing B16 melanoma. At 24 h, a tumor-to-blood ratio of as high as 37.3 ± 6.9 was attained (18). Several iodinated benzamide derivatives, including ¹²³I-BZA (19), *N*-(2-diethylaminoethyl)-2-¹²³I-iodobenzamide (20), ^{123/131}I-*N*-(2-diethylaminoethyl)-3-iodo-4-methoxybenzamide (21), and ¹²³I-2-hydroxy-3-iodo-6-methoxy-*N*-[(1-ethyl-2-pyrrolidinyl)methyl] benzamide (22), have been further studied in patients for melanoma imaging. These SPECT probes have shown promising results for clinical detection of melanoma lesions. Additionally, based on the structural elements of these benzamides, several ^{99m}Tc-complexes have also been designed and also display high uptake in melanoma tumors and excellent in vivo melanoma-imaging characteristics with SPECT in preclinical models (23,24). Very recently, a benzamide analog labeled with ¹⁸F was evaluated in a subcutaneous melanoma model and a biodistribution study demonstrated its promising tumor-targeting ability (25). Thus, the benzamide analogs are a reasonable starting point for the further development of melanin-targeted ¹⁸F-labeled probes.

¹⁸F is an ideal PET probe (half-life, 110 min; β^+ particles emitted at an energy of 635 keV; 97% abundant). In this study, an ¹⁸F-labeled benzamide analog, *N*-[2-(diethylamino)ethyl]-4-¹⁸F-fluorobenzamide (¹⁸F-FBZA), was synthesized and evaluated for melanin-targeted melanoma imaging.

MATERIALS AND METHODS

General

N-succinimidyl-4-fluorobenzoate (SFB) was purchased from ABX GmbH. All other chemicals, including *N,N*-diethylenediamine (DEDA), trifluoroacetic acid, *N,N'*-diisopropylethylamine, and acetonitrile (CH₃CN), were purchased from Sigma-Aldrich Chemical Co. The tumor cell lines and all instruments, including the electrospray ionization mass spectrometry, nuclear magnetic resonance, reverse-phase high-performance liquid chromatography (HPLC), and PET dose calibration equipment, were the same as described in our previous publication (26).

Synthesis of ^{18/19}F-FBZA

The nonradioactive reference standard ¹⁹F-FBZA was prepared by reaction of DEDA with SFB. Briefly, DEDA (9.8 mg) and SFB (5.3 mg) dissolved in 300 μ L of dimethyl sulfoxide and 5 μ L of *N,N'*-diisopropylethylamine were mixed and reacted for 80 min at 50°C. The reaction solution was injected into a semipreparative HPLC column for purification. The flow rate was 3 mL/min, with the mobile phase starting with 95% solvent A and 5% solvent B (0–3 min), going to 35% solvent A and 65% solvent B for 33 min, and then changing to 15% solvent A and 85% solvent B, which was maintained for another 3 min (36–39 min), followed by a return to the initial solvent composition by 42 min. Fractions containing the product were collected (retention time, 15.5 min) and yielded 70% of the desired compound, which was subsequently lyophilized and characterized by electrospray ionization

mass spectrometry or nuclear magnetic resonance. The measured molecular weight was consistent with the expected molecular weight: $m/z = 239.08$ measured for $[M+H]^+$ (C₁₃H₂₀FN₂O calculated molecular weight = 239.15); ¹H-nuclear magnetic resonance (400 MHz, dimethyl sulfoxide-*d*₆): δ 0.97 (quartet, 8H), 2.5 (s, 15H), 3.32 (t, 18H), 7.3 (dd, 2H), 7.9 (dd, 2H), 8.5 (t, 1H).

The radiofluorination synthon, ¹⁸F-SFB, was prepared according to a previously reported procedure (26). ¹⁸F-SFB (specific activity, 200–250 GBq/ μ mol) dissolved in 100 μ L of dimethyl sulfoxide was added to the DEDA (100 μ g) and *N,N'*-diisopropylethylamine (5 μ L) and reacted for 30 min at 50°C. The reaction solution was injected into an analytic HPLC column using the same elution gradient (flow rate, 1 mL/min) as for the synthesis of nonradioactive ¹⁹F-FBZA. The HPLC fractions containing the radiolabeled product ¹⁸F-FBZA were collected, combined, and evaporated with a rotary evaporator. The ¹⁸F-FBZA was reconstituted in phosphate-buffered saline and passed through a 0.22- μ m Millipore filter into a sterile vial for in vitro and in vivo animal experiments. The total radiosynthesis time for ¹⁸F-FBZA was 3 h, with an overall decay-corrected yield of 50% at the end of synthesis.

Serum Stability

The in vitro stability of ¹⁸F-FBZA was evaluated by incubation of 7.4 MBq (\sim 200 μ Ci) of probe with mouse serum (1 mL) at 37°C. At different times (30, 60, 120, and 150 min), the solution was filtered using a NanoSep 10 K centrifuge (Pall Corp.) to isolate low-molecular-weight metabolites. The filtrates were analyzed by reverse-phase HPLC under conditions identical to those used for analyzing original ¹⁸F-FBZA.

In Vitro Cell Uptake Studies

B16F10, A375M, and U87MG cells were cultured in Dulbecco's modified Eagle high-glucose medium (Gibco Life Sciences) supplemented with 10% fetal bovine serum with penicillin and streptomycin. The cells were regularly maintained in a 37°C, 5% CO₂ humidified incubator. The cellular uptake studies were performed on B16F10 cells. Briefly, about 1×10^6 B16F10 cells were plated in a 12-well plate and pretreated with 2 mM *L*-tyrosine for 24 h. The cells were then incubated with advanced modified Eagle's medium containing 25 mM *N*-(2-hydroxyethyl)piperazine-*N'*-(2-ethanesulfonic acid), 0.2% bovine serum albumin, and 0.3 mM 1,10-phenanthroline containing 3.7 kBq (0.1 μ Ci) of ¹⁸F-FBZA for 30 min, and for 120 min under either 37°C or 4°C. Nontreated cells were used as a control. The cells were then washed 3 times with ice-cold phosphate-buffered saline and lysed with 0.5 N NaOH for 5 min at room temperature. The radioactivity of the cell lysate was counted by a Wallac 1480 automated counter (Perkin Elmer). The counts per minute and percentage of uptake were plotted as a function of time using Prism 5.0 (GraphPad).

σ -Receptor Binding Assays

σ -receptor binding assays were conducted using standard methods detailed previously (27). The in vitro σ_1 -binding affinity of ¹⁹F-FBZA was determined in a competition assay using guinea pig brain membranes and the high-affinity σ_1 -ligand ³H-(+)-pentazocine. The σ_2 -receptor binding affinity of ¹⁹F-FBZA was determined using rat liver membrane preparations along with ³H-1,3-di-*o*-tolylguanidine as the radioligand in the presence of 10 μ M pentazocine to mask σ_1 -receptors. Competition assays were performed with 12 concentrations of ¹⁹F-FBZA ranging from 1×10^{-10} to 1×10^{-3} M and protein samples (0.15 mg of

membrane protein) in Tris-HCl (50 mM), pH 8.0, for 120 min at 25°C in a 0.25-mL volume.

Biodistribution

All animal studies were performed in compliance with the federal and local institutional rules for the conduct of animal experimentation. The subcutaneous tumor models were created with 5- to 6-wk-old male C57BL/6 mice (Charles River) for B16F10 and Nu/Foxn1 mice (Harlan) for A375M or U87MG. Pulmonary melanoma metastases were established in C57BL/6 mouse lungs via tail vein injection of 0.2×10^6 , 0.4×10^6 , or 0.8×10^6 B16F10 cells.

Biodistribution studies were conducted 1 or 2 h after tail vein injection of ^{18}F -FBZA in tumor-bearing mice (B16F10, A375M and U87MG; $n = 3$ each). The mice were sacrificed at 1 or 2 h after injection. Tumors, blood, and other major organs of interest were harvested, weighed, and counted in a Wallac 1480 automated counter. The results were expressed as %ID/g. To compare the melanoma-imaging abilities of ^{18}F -FBZA with ^{18}F -FDG, B16F10 mice were kept fasting overnight before the experiment. ^{18}F -FDG (3.7 MBq, 100 μCi) was injected via the tail vein of the B16F10 tumor-bearing mice, and small-animal PET and biodistribution experiments were performed 1 h after injection ($n = 5$).

In Vivo Imaging Procedure

PET of tumor-bearing mice was performed on an R4 rodent model scanner (Concord Microsystems). A group of mice ($n = 3$) bearing melanotic B16F10 was injected with ^{18}F -FBZA (3.31–3.86 MBq [89.4–104.3 μCi]) via the tail vein. For the amelanotic A375M tumors ($n = 3$), 0.87–0.95 MBq (23.6–25.8 μCi) of the probe was injected, whereas for U87MG tumors ($n = 3$), 0.29–0.4 MBq (7.95–10.93 μCi) of ^{18}F -FBZA was injected. At 1 and 2 h after injection, the mice were anesthetized with 2% isoflurane (AErrane; Baxter) and placed prone near the center of the field of view of the scanner. For ^{18}F -FDG studies, a 3.7-MBq (100- μCi) dose of ^{18}F -FDG was injected via the tail vein. Five-minute static scans were obtained, and the images were reconstructed using a 2-dimensional ordered-subsets expectation maximum algorithm.

Respiratory gated micro-CT images were acquired using an in vivo scanner (eXplore Locus; GE Healthcare). Immediately after the PET scan, the mice were transported to and positioned in the CT scanner while still fixed to their polystyrene bed containing 4 fiducial markers at different positions. The mice were sedated with 2% isoflurane during the scan. The micro-CT images were acquired with the x-ray source set at 70 kVp and 40 μA and synchronized by respiratory gating on a Biovet system. CT images were reconstructed using a fanbeam re-sorting algorithm with a standard ramp filter. Images were reconstructed on a 512×512 pixel grid with a pixel size of $49 \times 49 \mu\text{m}$. No radiographic contrast medium was used.

PET images were imported using ASIPro VM (Concorde Microsystems). Regions of interest (ROIs) were drawn manually over the tumor or organ of interest on decay-corrected whole-body coronal images. The mean counts per pixel per minute were

obtained from the ROIs and converted to counts per milliliter per minute using a calibration constant. No attenuation correction was performed. CT images were imported using MicroView (version 2.1.2; GE Healthcare). For coregistration with PET datasets, the fiducial markers were aligned using a wizard in the nonproprietary AMIDE software, version 0.9.1 (28).

Statistical Methods

Statistical analysis was performed using the Student *t* test for unpaired data. A 95% confidence level was chosen to determine the significance of differences between groups, with a *P* value of less than 0.05 indicating a significant difference.

RESULTS

Chemistry and Radiochemistry

The nonradioactive ^{19}F -FBZA was synthesized in a 1-step coupling reaction between DEDA and SFB (Fig. 1). HPLC purification of the nonradioactive ^{19}F -FBZA yielded approximately 70% of the desired product with a 15.5-min retention time. The identity of the isolated compound was subsequently verified and confirmed by electro-spray ionization mass spectrometry and nuclear magnetic resonance.

Similarly, radiosynthesis of ^{18}F -FBZA was achieved through coupling of the radiosynthon, ^{18}F -SFB, with the amino group of DEDA. The procedure and radiochemical synthetic module for production of the radiosynthon ^{18}F -SFB have been well established in our radiochemistry facility, and ^{18}F -SFB has been successfully used and described in our earlier work for ^{18}F -labeling of a peptide for melanoma imaging (26). The total time for radiosynthesis of ^{18}F -FBZA was approximately 3 h. The maximum overall radiochemical yield with decay correction was 50%, and the specific activity of ^{18}F -FBZA was estimated to be 132–166 GBq/ μmol at the end of synthesis. The radiochemical purity of the product was greater than 95% as verified by analytic HPLC analysis (Fig. 2A). The authenticity of ^{18}F -FBZA was verified by coinjection with the previously characterized nonradioactive ^{19}F -FBZA. Both cold and radioactive FBZA compounds displayed similar HPLC retention times.

Serum Stability of ^{18}F -FBZA

^{18}F -FBZA displayed good stability in mouse serum (Fig. 2B). The percentage of intact probe was 94.1%, 93.5%, 87.8%, and 85.1% at 30, 60, 120, and 150 min of incubation, respectively. Defluorination was not observed for ^{18}F -FBZA incubated with mouse serum up to 150 min. Overall, ^{18}F -FBZA can be reliably produced and demonstrates good in vitro stability.

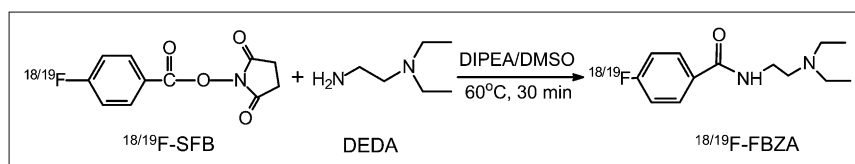


FIGURE 1. Synthetic scheme for preparation of $^{18/19}\text{F}$ -FBZA.

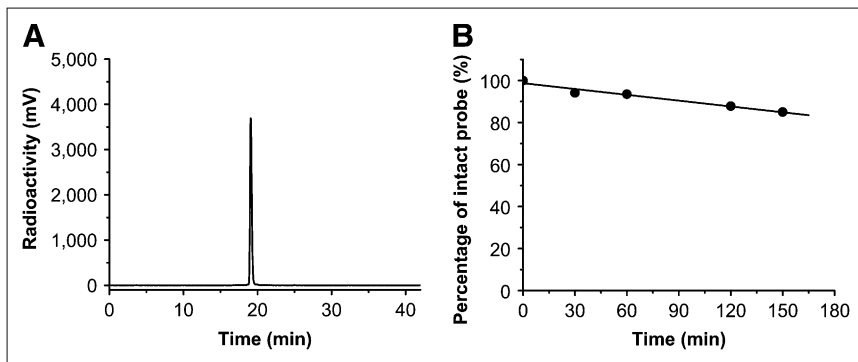


FIGURE 2. HPLC radiochromatogram of purified ^{18}F -FBZA (A), and in vitro mouse serum stability study of ^{18}F -FBZA (B).

Cell Uptake of ^{18}F -FBZA

The B16F10 cell uptake of ^{18}F -FBZA over a 2-h incubation period at 4°C and 37°C (Fig. 3) was $0.49\% \pm 0.03\%$ and $0.52\% \pm 0.1\%$, respectively. Pretreatment of the B16F10 cells with L-tyrosine (2.0 mM) for 24 h significantly darkened B16F10 cells, compared with control cells. These tyrosine-stimulated cells displayed a significantly enhanced accumulation of ^{18}F -FBZA at both 4°C and 37°C ($P < 0.001$). At 37°C (Fig. 3B), within 30 min of incubation the tyrosine-stimulated cells maximized at $10.7\% \pm 0.8\%$ uptake of ^{18}F -FBZA and remained at 8.1 ± 1.9 at 2 h, which amounts to an 18- to 25-fold increase compared with uptake by the nontreated B16F10 cells. At 4°C (Fig. 3A), the uptake maximized at 30 min with $4.5\% \pm 0.5\%$ accumulation, which was 58% less than uptake at 37°C ($P < 0.05$).

σ -Receptor-Binding Studies of ^{19}F -FBZA

Benzamide analogs have previously been shown to possess high binding affinity with σ -receptors, which are normally overexpressed in melanoma cells (27,29). To gain a better understanding of the involvement of σ -receptor binding of ^{18}F -FBZA in the uptake of FBZA in melanoma cells, we further measured the binding affinity of the nonradioactive ^{19}F -FBZA in established σ -receptor assays using guinea-pig brain (σ_1 -receptor) and rat liver membrane (σ_2 -receptor)

preparations (24). These assays showed that ^{19}F -FBZA displays low affinity toward either σ_1 -receptor (inhibition constant, $8.90 \mu\text{M}$) or σ_2 -receptor (inhibition constant, 0.12 mM).

Biodistribution

The in vivo biodistribution of ^{18}F -FBZA was examined in B16F10 murine allografts, as well as in A375M and U87MG xenografts. In biodistribution studies of ^{18}F -FBZA performed at 1 and 2 h in the B16F10 model, ^{18}F -FBZA displayed a significant uptake in the melanotic B16F10 melanoma allograft, with 6.47 ± 2.16 and 5.94 ± 1.83 %ID/g at 1 and 2 h, respectively (Table 1; Supplemental Fig. 1 [supplemental materials are available online only at <http://jnm.snmjournals.org>]). At 2 h, the tumor-to-blood ratio was 34.0 ± 13.2 and the tumor-to-muscle ratio was 23.3 ± 10.1 . The in vivo biodistribution of ^{18}F -FBZA in the A375M and U87MG mouse models, however, was low, with tumor uptake of 0.75 ± 0.09 and 0.56 ± 0.13 %ID/g and tumor-to-blood ratios of 4.70 ± 0.78 and 3.57 ± 1.34 , respectively (Table 1; Supplemental Fig. 1).

In the B16F10 pulmonary metastasis model, the mice were sacrificed 13 d after intravenous inoculation of B16F10 cells. In the 2 groups of mice ($n = 3$ each) (0.2 and 0.4×10^6 B16F10 tumor cells), biodistribution and small-animal PET studies showed that the radioactivity in melanoma

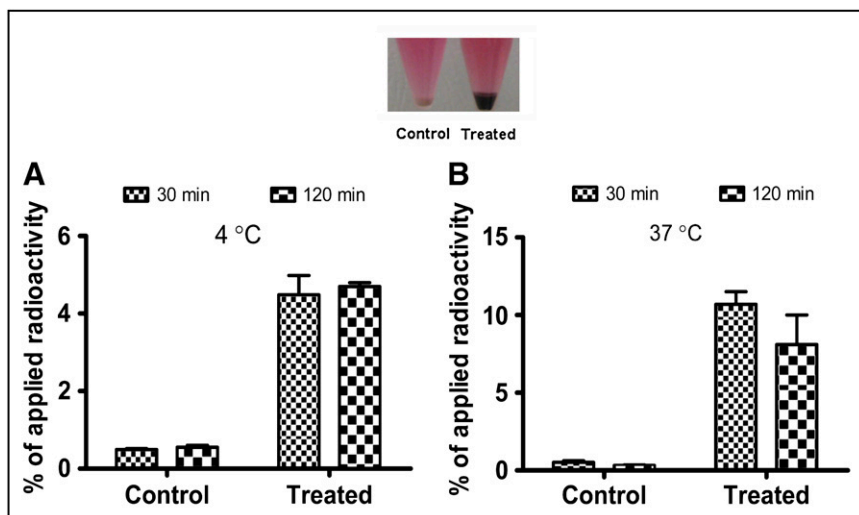


FIGURE 3. In vitro cell uptake of ^{18}F -FBZA. Digital photo is shown of B16F10 cell pellet with (right) or without (left) L-tyrosine treatment for 24 h at 4°C (A) and 37°C (B). Data are expressed as mean \pm SD, with each data point representing triplicate study.

TABLE 1. Biodistribution Results of Different Tumor-Bearing Mice

Organ	¹⁸ F-FBZA %ID/g at 2 h in...			In B16F10 at 1 h, %ID/g of...	
	A375M (n = 3)	U87MG (n = 3)	B16F10 (n = 3)	¹⁸ F-FBZA (n = 3)	¹⁸ F-FDG (n = 5)
Tumor	0.75 ± 0.09	0.56 ± 0.13	5.94 ± 1.83	6.47 ± 2.16	9.46 ± 2.56
Blood	0.16 ± 0.04	0.16 ± 0.04	0.18 ± 0.04	0.72 ± 0.17	1.18 ± 0.31
Heart	0.35 ± 0.12	0.41 ± 0.03	0.37 ± 0.08	1.62 ± 0.33	54.36 ± 13.15
Liver	2.82 ± 0.46	2.81 ± 0.70	3.07 ± 0.18	8.82 ± 2.13	1.81 ± 0.61
Lung	0.82 ± 0.24	0.82 ± 0.42	0.85 ± 0.23	2.92 ± 0.40	7.61 ± 1.53
Kidney	1.04 ± 0.25	1.14 ± 0.49	0.93 ± 0.26	6.99 ± 3.13	7.43 ± 2.64
Muscle	0.34 ± 0.11	0.33 ± 0.07	0.27 ± 0.05	1.26 ± 0.14	1.81 ± 0.69
Spleen	0.57 ± 0.18	1.17 ± 0.55	0.36 ± 0.05	2.45 ± 0.51	5.39 ± 0.90
Brain	0.47 ± 0.05	0.38 ± 0.05	0.35 ± 0.05	1.71 ± 0.06	3.18 ± 0.58
Intestine	0.83 ± 0.45	1.13 ± 0.56	0.75 ± 0.18	3.04 ± 0.24	4.34 ± 0.97
Stomach	1.24 ± 0.46	0.91 ± 0.55	1.21 ± 0.92	5.26 ± 0.79	3.10 ± 0.87
Pancreas	0.64 ± 0.24	0.89 ± 0.41	0.51 ± 0.12	3.70 ± 1.22	3.14 ± 0.85
Bone	0.21 ± 0.10	0.44 ± 0.07	0.51 ± 0.03	1.22 ± 0.18	4.30 ± 2.45
Eyes	0.31 ± 0.10	0.30 ± 0.03	17.80 ± 1.72	18.11 ± 3.48	6.48 ± 2.33
Skin	0.53 ± 0.14	0.66 ± 0.03	0.33 ± 0.05	1.56 ± 0.65	2.00 ± 0.49
Uptake ratio					
Tumor-to-blood	4.70 ± 0.78	3.57 ± 1.34	33.95 ± 13.24	9.50 ± 4.53	8.59 ± 3.22
Tumor-to-muscle	2.31 ± 0.50	1.71 ± 0.44	23.33 ± 10.10	5.20 ± 2.06	5.65 ± 1.84

lung metastases reached 10.0 ± 3.92 and 7.87 ± 3.56 %ID/g, respectively, at 2 h after injection (Table 2). In normal lung tissue, the probe accumulation was 0.99 ± 0.04 %ID/g at 2 h after injection (Table 2)—a value that was similar to that observed in the B16F10 subcutaneous model, in which the normal-lung uptake was 0.85 ± 0.23 %ID/g at 2 h. The lung-to-blood ratios for the pulmonary metastasis model were 24.7 ± 13.5 and 38.9 ± 10.3 , respectively. The lung-to-blood ratio for the B16F10 subcutaneous model was 4.72 ± 0.46 , whereas 4.23 ± 0.66 was observed in control C57BL6 mice at 2 h. Both absolute lung uptake and lung-to-blood ratio were significantly higher for the pulmonary metastasis model than for the subcutaneous model or for control C57BL6 mice ($P < 0.01$).

To further explore the translational potential of ¹⁸F-FBZA in melanoma imaging, we compared ¹⁸F-FBZA and ¹⁸F-FDG (Table 1). ¹⁸F-FDG uptake by the B16F10 tumor was high at 1 h and was not significantly different from ¹⁸F-FBZA uptake in the same tumor model. Lung uptake was 7.61 ± 1.53 and 2.92 ± 0.40 %ID/g for ¹⁸F-FDG and ¹⁸F-FBZA, respectively, suggesting much higher normal-lung uptake of ¹⁸F-FDG ($P < 0.01$). Heart uptake of ¹⁸F-FDG was significantly higher than that of ¹⁸F-FBZA ($P < 0.01$). However, liver uptake of ¹⁸F-FDG was lower than that of ¹⁸F-FBZA at 1 h after injection ($P < 0.05$).

Imaging Studies

In static small-animal PET images (Fig. 4A), B16F10 tumors were clearly visualized at 1 h with good tumor-to-

TABLE 2. Biodistribution Results of ¹⁸F-FBZA in Normal Mice and B16F10-Bearing Mice at 2 Hours After Injection

Organ	Normal mice	Mice bearing B16F10	
		0.2×10^6 cells (n = 3)	0.4×10^6 cells (n = 3)
Lung	0.99 ± 0.04	10.00 ± 3.92	7.87 ± 3.56
Blood	0.24 ± 0.03	0.42 ± 0.24	0.20 ± 0.06
Heart	0.64 ± 0.02	0.43 ± 0.02	0.47 ± 0.15
Liver	3.11 ± 0.41	3.15 ± 0.39	3.73 ± 0.80
Kidney	1.80 ± 0.13	1.29 ± 0.93	1.42 ± 0.24
Muscle	0.63 ± 0.21	0.46 ± 0.14	0.42 ± 0.09
Spleen	0.87 ± 0.02	0.54 ± 0.18	0.75 ± 0.22
Brain	0.61 ± 0.03	0.48 ± 0.14	0.35 ± 0.06
Intestine	0.98 ± 0.07	0.69 ± 0.17	1.02 ± 0.29
Stomach	2.24 ± 0.53	1.21 ± 0.48	1.48 ± 0.24
Pancreas	0.65 ± 0.28	0.60 ± 0.25	0.80 ± 0.25
Bone	0.71 ± 0.10	0.58 ± 0.12	0.61 ± 0.06
Uptake ratio			
Lung-to-blood	4.23 ± 0.66	24.67 ± 13.53	38.90 ± 10.37
Lung-to-liver	0.30 ± 0.03	2.25 ± 1.26	2.08 ± 0.69

Tracer was injected 13 d after injection of the stated number of cells. Data are %ID/g.

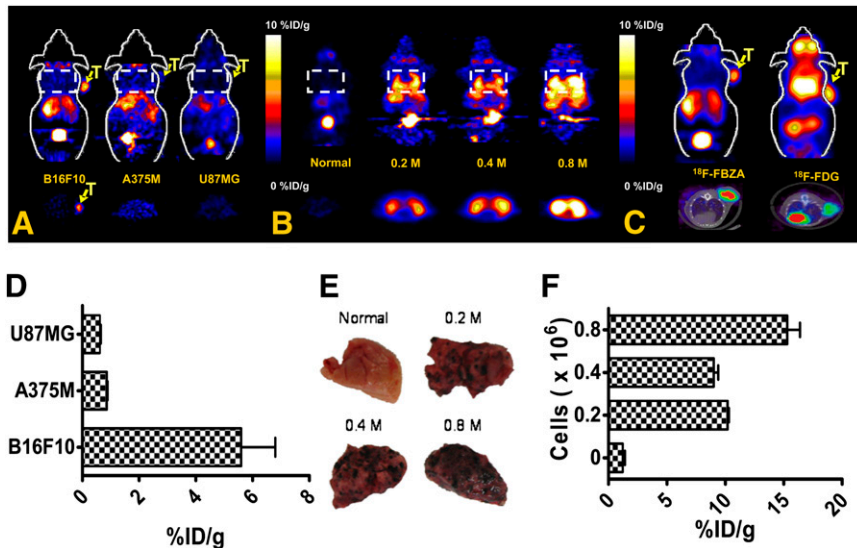


FIGURE 4. (A) Representative decay-corrected coronal (top) and transaxial (bottom) small-animal ^{18}F -FBZA PET images of B16F10, A375M, and U87MG subcutaneous tumor models. Tumor locations (T) and lung regions (rectangles) are indicated. (B) Representative decay-corrected coronal (top) and transaxial (bottom) small-animal PET images of B16F10 melanoma lung metastasis model that was established 13 d after tail vein injection of 0.2×10^6 ($n = 3$), 0.4×10^6 ($n = 3$), or 0.8×10^6 ($n = 2$) B16F10 cells. (C) Representative decay-corrected small-animal PET coronal images (top) and small-animal PET/CT fusion transaxial images (bottom) of C57BL/6 mice bearing B16F10 tumors. (D) Quantification analysis of tumor uptake of ^{18}F -FBZA in different models for comparison. (E) Photographs of biopsy samples of lung metastases. (F) Quantification analysis of ^{18}F -FBZA uptake by melanoma lung metastases.

background contrast (see Supplemental Fig. 2 for dynamic scan), whereas for A375M and U87MG, tumor uptake was hardly visible. Liver and kidney uptake was visualized in all animals. ROI analysis of tumor uptake showed that B16F10 had significantly higher tumor uptake (5.6 ± 1.2 %ID/g) than did the other 2 tumor types (0.86 ± 0.03 and 0.61 ± 0.04 %ID/g for A375M and U87MG, respectively) (Fig. 4D) ($P < 0.01$).

In vivo studies with the lung metastasis model, compared with the normal lung, clearly showed a region of symmetric uptake greater than the background level in the chest of mice bearing pulmonary metastases (Fig. 4B). ROI analysis showed that normal-lung uptake of ^{18}F -FBZA was 1.2 ± 0.2 %ID/g whereas uptake of 10.2 ± 0.1 , 9.0 ± 0.4 , and 15.3 ± 1.1 %ID/g was observed for lungs harboring metastases resulting from tumor doses of 0.2, 0.4, or 0.8×10^6 B16F10 cells, respectively (Fig. 4F).

In vivo small-animal PET of the subcutaneous B16F10 melanoma using ^{18}F -FBZA or ^{18}F -FDG showed that the 2 agents have different biodistribution patterns (Fig. 4C). For ^{18}F -FBZA, radioactivity accumulation in tumor and liver is observed as washout through the kidneys into the bladder. ^{18}F -FDG, on the other hand, accumulated in the heart, eyes, (Harderian glands), and tumor, whereas liver activity was low. PET ROI analyses showed that tumor uptake for ^{18}F -FBZA was 5.6 ± 1.2 whereas that for ^{18}F -FDG was 6.31 ± 0.61 %ID/g ($P > 0.05$). PET/CT fusion images clearly demonstrated the tumor anatomy and specific tumor uptake of the different probes.

DISCUSSION

Malignant melanoma is well known for its aggressiveness and strong metastatic potential, and early detection and identification of metastasis can improve management

and prognosis. The lethality of malignant melanoma is caused mostly by metastasis to distant organs, mainly the lungs, liver, brain, and soft tissues. Monoclonal antibodies against high-molecular-weight melanoma-associated antigens (30,31) or peptides targeting melanocortin receptor 1 (26,32) have been labeled with various radioisotopes for radioimmunodetection and radioimmunotherapy of malignant melanoma and its metastases. Melanin-binding peptides and antibodies are also used to target melanin and have achieved therapeutic effects in melanoma animal models (17,33,34). Though antibody and peptide-based approaches successfully target the primary tumor in many melanoma models, limitations include relatively slow and low tumor uptake, high kidney uptake, and in vivo instability, among others (17).

Compared with peptide-based probes, a group of molecules with coplanar fused rings has been shown to bind strongly with melanin (35). Particularly, benzamide-based small molecules can specifically target the melanotic melanomas and their metastases, as evidenced by numerous studies of radioiodinated benzamide analogs (19). In a limited clinical trial, the sensitivity and specificity of ^{123}I -BZA were 100% and 81%, respectively (36). Very recently, a ^{125}I -labeled BZA derivative was developed and showed high specificity and long tumor retention times—16-fold higher than for ^{125}I -BZA at 72 h after injection—making it a promising radiopharmaceutical for targeted radionuclide therapy of melanoma (37). With the development of diagnostic PET and its high sensitivity, an ^{18}F PET probe based on BZA molecules may improve the sensitivity of detection and diagnosis of melanotic melanoma and its metastasis.

An ^{18}F -labeled benzamide, ^{18}F -FBZA, was thus successfully synthesized and evaluated in cultured cells and tumor-bearing mice. In vitro cellular uptake studies showed

that treatment of B16F10 cells with L-tyrosine (2 mM) substantially increased ^{18}F -FBZA uptake from $0.32\% \pm 0.04\%$ to $8.1\% \pm 1.9\%$ at 37°C at 2 h, indicating that maximal ^{18}F -FBZA uptake is associated with melanin content (Fig. 3). Earlier reports on cell culture studies and in vivo scintigraphic imaging with ^{123}I -*N*-(2-diethylaminoethyl)-4-iodobenzamide suggested that σ_1 - and σ_2 -receptors might play an important role in uptake of benzamides, possibly attributable to the neuroectodermal origin of melanoma (38); however, the low σ -receptor affinity displayed by ^{19}F -FBZA suggests that σ -receptors do not play a role in B16F10 uptake of this probe. This observation, coupled with the observation that cellular uptake for the ^{18}F -FBZA probe at 4°C was significantly increased after tyrosine pretreatment, cannot be explained by receptor-mediated endocytosis. Alternatively, uptake of radioiodinated benzamides by melanoma has previously been observed and shown to be related to the melanin content of the cells (39). Labarre et al. have also shown that a complex interaction between BZA and melanin involves both ionic and hydrophobic binding sites (39). In addition, studies with melanoma-targeting $^{99\text{m}}\text{Tc}$ -complexes designed to mimic and contain the structural elements of BZA have also been shown to target melanoma on the basis of the melanin content of the tumors (29,40). Taken together, these findings indicate that uptake and accumulation in melanotic B16F10 cells of the neutral, lipophilic ^{18}F -FBZA are caused by its passive diffusion through cell membranes into cytoplasm, followed by binding with melanin structures and trapping within cells.

In vivo studies used the B16F10 melanotic melanoma along with the amelanotic A375M melanoma and the human glioblastoma U87MG as control tumors. The in vivo tumor uptake of ^{18}F -FBZA in B16F10 reached 6.47 ± 2.16 %ID/g at 1 h and remained high up to 2 h after injection. In contrast, the in vivo tumor uptake of ^{18}F -FBZA by A375M attained only 0.75 ± 0.09 %ID/g, and U87MG also displayed a low tumor uptake of 0.56 ± 0.13 %ID/g at 2 h, both being significantly lower than the uptake observed for the melanotic B16F10 tumors ($P < 0.01$) (Table 1). Taken together with the in vitro cellular uptake assay, the in vivo results further prove that the target of ^{18}F -FBZA binding is melanin within the melanoma.

Analysis of the in vivo results also reveals no significant difference in the uptake and distribution of ^{18}F -FBZA in other nontarget organs among B16F10, A375M, and U87MG in vivo tumor models (Table 1) ($P > 0.05$). Given the higher tumor uptake in B16F10 melanotic melanoma, the tumor-to-normal-organ ratios are thus significantly higher for the B16F10 model ($P < 0.01$), indicating that ^{18}F -FBZA has an excellent in vivo tumor targeting ability for melanotic melanoma. In view of the high incidence (88%) of melanotic malignant melanoma, ^{18}F -FBZA represents a potentially viable PET probe for clinical studies of metastasis of malignant melanoma (41).

A goal of these studies was to explore the feasibility of using ^{18}F -FBZA in the early detection of melanoma

metastases. This goal was accomplished using the preclinical pulmonary metastasis melanoma model, in which we found that melanotic pulmonary lesions of B16F10 tumors specifically accumulated ^{18}F -FBZA (Table 2; Fig. 4). Lung uptake in this B16F10 model was significantly higher than lung uptake of ^{18}F -FBZA in the B16F10 subcutaneous model lacking pulmonary metastases or in control C57BL/6 mice ($P < 0.05$). Regarding ^{18}F -FDG uptake in the chest, the values were 7.61 ± 1.53 %ID/g in the lung and more than 50 %ID/g in the heart, both of which can interfere with the delineation of melanotic lung lesions and thus limit the use of ^{18}F -FDG for detection of pulmonary metastasis in melanoma (Table 1; Fig. 4C). In small-animal PET images, there was significantly higher lung uptake, shown by symmetric hot regions in the mouse chest bearing B16F10 pulmonary metastases. The individual metastatic lesions were smaller than the resolution of the small-animal PET scanner. That consideration, plus motion of the lung, prevented single micrometastasis from being discernable using small-animal PET (Fig. 4B).

Interestingly, brain uptake in the B16F10 model reached about 1.71 ± 0.06 and 0.35 ± 0.05 %ID/g at 1 and 2 h, respectively, after injection (Table 1), suggesting that the probe could pass the blood-brain barrier. The tumor-to-brain ratio at 1 h for ^{18}F -FBZA reached 5.14 ± 1.10 , compared with the lower value of 2.86 ± 0.35 for ^{18}F -FDG that is due to the high normal-brain uptake of ^{18}F -FDG. These results also demonstrated the potential of using ^{18}F -FBZA for imaging melanoma brain metastases. However, uptake in melanized neurons remains to be addressed. Additionally, ^{18}F -FBZA accumulates in the melanin-containing eyes (retinas) of normal C57BL/6 mice but not in the pink eyes of nude mice (Table 1; Supplemental Fig. 3), further suggesting the capability of cellular penetration and binding to melanin structures by ^{18}F -FBZA.

In further comparing ^{18}F -FBZA with ^{18}F -FDG, we found that subcutaneous tumor uptake at both 1 and 2 h for ^{18}F -FBZA was comparable to that for ^{18}F -FDG at 1 h ($P > 0.05$). However, given the presence of phosphatases in the liver, the liver uptake at 1 h was much lower for ^{18}F -FDG than for ^{18}F -FBZA ($P < 0.05$). Kidney uptake is another major concern for radiopharmaceuticals, the kidney being a radiosensitive organ. Although there was no significant difference in kidney uptake of ^{18}F -FBZA and ^{18}F -FDG at 1 h, kidney uptake of ^{18}F -FBZA decreased from 1 to 2 h—from 6.99 ± 3.13 to 0.93 ± 0.26 %ID/g—suggesting faster clearance of the ^{18}F -FBZA probe.

CONCLUSION

A novel ^{18}F -labeled PET probe, ^{18}F -FBZA, was successfully synthesized via a 1-step conjugation reaction between the radiosynthon, ^{18}F -SFB, and DEDA. ^{18}F -FBZA specifically targeted both primary and pulmonary melanotic metastatic lesions with high tumor uptake and good tumor-to-normal-tissue ratios. These findings, taken together,

show that ^{18}F -FBZA represents a potential PET probe for imaging melanotic malignant melanoma and its metastases.

ACKNOWLEDGMENTS

This work was supported, in part, by the Melanoma Research Alliance, grant R24 CA93862 from the Small Animal Imaging Resource Program of the National Cancer Institute, and grant P50 CA114747 from the *In Vivo* Cellular Molecular Imaging Center of the National Cancer Institute. We thank Carsten Nielsen for help with CT data acquisition.

REFERENCES

1. Jemal A, Siegel R, Ward E, Hao Y, Xu J, Thun MJ. Cancer statistics, 2009. *CA Cancer J Clin.* 2009;59:225–249.
2. Thompson JF, Scolyer RA, Kefford RF. Cutaneous melanoma. *Lancet.* 2005;365:687–701.
3. Belhocine TZ, Scott AM, Even-Sapir E, Urbain JL, Essner R. Role of nuclear medicine in the management of cutaneous malignant melanoma. *J Nucl Med.* 2006;47:957–967.
4. Prichard RS, Hill AD, Skehan SJ, O'Higgins NJ. Positron emission tomography for staging and management of malignant melanoma. *Br J Surg.* 2002;89:389–396.
5. Choi EA, Gershenwald JE. Imaging studies in patients with melanoma. *Surg Oncol Clin N Am.* 2007;16:403–430.
6. Dimitrakopoulou-Strauss A, Strauss LG, Burger C. Quantitative PET studies in pretreated melanoma patients: a comparison of 6- ^{18}F fluoro-L-dopa with ^{18}F -FDG and ^{15}O -water using compartment and noncompartment analysis. *J Nucl Med.* 2001;42:248–256.
7. Lindholm P, Leskinen S, Nagren K, et al. Carbon-11-methionine PET imaging of malignant melanoma. *J Nucl Med.* 1995;36:1806–1810.
8. Cobben DC, Jager PL, Elsinga PH, Maas B, Suurmeijer AJ, Hoekstra HJ. 3'- ^{18}F -fluoro-3'-deoxy-L-thymidine: a new tracer for staging metastatic melanoma? *J Nucl Med.* 2003;44:1927–1932.
9. Beer AJ, Haubner R, Goebel M, et al. Biodistribution and pharmacokinetics of the alphavbeta3-selective tracer ^{18}F -galacto-RGD in cancer patients. *J Nucl Med.* 2005;46:1333–1341.
10. Gambhir SS. Molecular imaging of cancer with positron emission tomography. *Nat Rev Cancer.* 2002;2:683–693.
11. Jimbow K, Miyake Y, Homma K, et al. Characterization of melanogenesis and morphogenesis of melanosomes by physicochemical properties of melanin and melanosomes in malignant melanoma. *Cancer Res.* 1984;44:1128–1134.
12. Prota G. Melanins, melanogenesis and melanocytes: looking at their functional significance from the chemist's viewpoint. *Pigment Cell Res.* 2000;13:283–293.
13. Iozumi K, Hoganson GE, Pennella R, Everett MA, Fuller BB. Role of tyrosinase as the determinant of pigmentation in cultured human melanocytes. *J Invest Dermatol.* 1993;100:806–811.
14. Pankovich JM, Jimbow K. Tyrosine transport in a human melanoma cell line as a basis for selective transport of cytotoxic analogues. *Biochem J.* 1991;280:721–725.
15. Jimbow K, Miura T, Ito S, Ishikawa K. Phenolic melanin precursors provide a rational approach to the design of antitumor agents for melanoma. *Pigment Cell Res.* 1989;2:34–39.
16. Desbois N, Gardette M, Papon J, et al. Design, synthesis and preliminary biological evaluation of acridine compounds as potential agents for a combined targeted chemo-radiation therapy approach to melanoma. *Bioorg Med Chem.* 2008;16:7671–7690.
17. Dadachova E, Moadel T, Schweitzer AD, et al. Radiolabeled melanin-binding peptides are safe and effective in treatment of human pigmented melanoma in a mouse model of disease. *Cancer Biother Radiopharm.* 2006;21:117–129.
18. Michelot JM, Moreau MF, Labarre PG, et al. Synthesis and evaluation of new iodine-125 radiopharmaceuticals as potential tracers for malignant melanoma. *J Nucl Med.* 1991;32:1573–1580.
19. Michelot JM, Moreau MF, Veyre AJ, et al. Phase II scintigraphic clinical trial of malignant melanoma and metastases with iodine-123-N-(2-diethylaminoethyl 4-iodobenzamide). *J Nucl Med.* 1993;34:1260–1266.
20. Moins N, D'Incan M, Bonafous J, et al. ^{123}I -N-(2-diethylaminoethyl)-2-iodobenzamide: a potential imaging agent for cutaneous melanoma staging. *Eur J Nucl Med Mol Imaging.* 2002;29:1478–1484.
21. Nicholl C, Mohammed A, Hull WE, Bubeck B, Eisenhut M. Pharmacokinetics of iodine-123-IMBA for melanoma imaging. *J Nucl Med.* 1997;38:127–133.
22. Maffioli L, Mascheroni L, Mongioj V, et al. Scintigraphic detection of melanoma metastases with a radiolabeled benzamide ([iodine-123]-(S)-IBZM). *J Nucl Med.* 1994;35:1741–1747.
23. Cheng Z, Mahmood A, Li H, Davison A, Jones AG. [$^{99\text{m}}\text{Tc}$ COAADT]-(CH₂)₂-NEt₂: a potential small-molecule single-photon emission computed tomography probe for imaging metastatic melanoma. *Cancer Res.* 2005;65:4979–4986.
24. Friebe M, Mahmood A, Bolzati C, et al. [$^{99\text{m}}\text{Tc}$]oxotechnetium(V) complexes amine-amide-dithiol chelates with dialkylaminoalkyl substituents as potential diagnostic probes for malignant melanoma. *J Med Chem.* 2001;44:3132–3140.
25. Garg S, Kothari K, Thopate SR, Doke AK, Garg PK. Design, synthesis, and preliminary in vitro and in vivo evaluation of N-(2-diethylaminoethyl)-4- ^{18}F -fluorobenzamide ^{18}F -DAFBA: a novel potential PET probe to image melanoma tumors. *Bioconjug Chem.* February 17, 2009 [Epub ahead of print].
26. Cheng Z, Zhang L, Graves E, et al. Small-animal PET of melanocortin 1 receptor expression using a ^{18}F -labeled alpha-melanocyte-stimulating hormone analog. *J Nucl Med.* 2007;48:987–994.
27. Eisenhut M, Mohammed A, Mier W, et al. Melanoma uptake of $^{99\text{m}}\text{Tc}$ complexes containing the N-(2-diethylaminoethyl)benzamide structural element. *J Med Chem.* 2002;45:5802–5805.
28. Loening AM, Gambhir SS. AMIDE: a free software tool for multimodality medical image analysis. *Mol Imaging.* 2003;2:131–137.
29. Pham TQ, Greguric I, Liu X, et al. Synthesis and evaluation of novel radioiodinated benzamides for malignant melanoma. *J Med Chem.* 2007;50:3561–3572.
30. Matzku S, Kirchgessner H, Schmid U, Temponi M, Ferrone S. Melanoma targeting with a cocktail of monoclonal antibodies to distinct determinants of the human HMW-MAA. *J Nucl Med.* 1989;30:390–397.
31. Larson SM, Carrasquillo JA, McGuffin RW, et al. Use of I-131 labeled, murine Fab against a high molecular weight antigen of human melanoma: preliminary experience. *Radiology.* 1985;155:487–492.
32. Cheng Z, Chen J, Quinn TP, Jurisson SS. Radioiodination of rhenium cyclized alpha-melanocyte-stimulating hormone resulting in enhanced radioactivity localization and retention in melanoma. *Cancer Res.* 2004;64:1411–1418.
33. Dadachova E, Nosanchuk JD, Shi L, et al. Dead cells in melanoma tumors provide abundant antigen for targeted delivery of ionizing radiation by a mAb to melanin. *Proc Natl Acad Sci USA.* 2004;101:14865–14870.
34. Revskaya E, Jongco AM, Sellers RS, et al. Radioimmunotherapy of experimental human metastatic melanoma with melanin-binding antibodies and in combination with dacarbazine. *Clin Cancer Res.* 2009;15:2373–2379.
35. Ings RM. The melanin binding of drugs and its implications. *Drug Metab Rev.* 1984;15:1183–1212.
36. Chezal JM, Papon J, Labarre P, et al. Evaluation of radiolabeled (hetero)aromatic analogues of N-(2-diethylaminoethyl)-4-iodobenzamide for imaging and targeted radionuclide therapy of melanoma. *J Med Chem.* 2008;51:3133–3144.
37. Everaert H, Flamen P, Franken PR, Verhaeghe W, Bossuyt A. Sigma-receptor imaging by means of I123-IDAB scintigraphy: clinical application in melanoma and non-small cell lung cancer. *Anticancer Res.* 1997;17:1577–1582.
38. Eisenhut M, Hull WE, Mohammed A, et al. Radioiodinated N-(2-diethylaminoethyl)benzamide derivatives with high melanoma uptake: structure-affinity relationships, metabolic fate, and intracellular localization. *J Med Chem.* 2000;43:3913–3922.
39. Labarre P, Papon J, Moreau MF, et al. Melanin affinity of N-(2-diethylaminoethyl)-4-iodobenzamide, an effective melanoma imaging agent. *Melanoma Res.* 2002;12:115–121.
40. Limpa-Amara NMA, Zhu A, Cheng Z, Zimmerman RE, Jones AG. Comparative evaluation of a $^{99\text{m}}\text{Tc}$ -labeled tertiary amine complex and [^{18}F]-FDG as probes for imaging melanoma metastasis in mice [abstract]. *J Nucl Med.* 2005;46 (suppl):400P.
41. Velez A, Walsh D, Karakousis CP. Treatment of unknown primary melanoma. *Cancer.* 1991;68:2579–2581.